AIMS Mathematics, 10(9): 21835–21852.
DOI: 10.3934/math.2025971
Received: 07 July 2025
Revised: 08 September 2025
Accepted: 11 September 2025
Published: 19 September 2025

https://www.aimspress.com/journal/Math

*Research article*

# On symmetric potential in a boundary value problem dependent on an eigenparameter

**Elif Başkaya**[1] **and Süleyman Şengül**[2,*]

[1] Department of Mathematics, Faculty of Science, Karadeniz Technical University, Trabzon 61080, Türkiye

[2] Department of Mathematics, Faculty of Arts and Sciences, Recep Tayyip Erdoğan University, Rize 53100, Türkiye

* **Correspondence:** Email: suleyman.sengul@erdogan.edu.tr.

**Abstract:** In this work, we asymptotically calculate the eigenvalue of a boundary value problem that involves an integrable and symmetric potential over a defined interval and includes eigenvalues in the boundary conditions. We apply the Riccati equation to derive the asymptotic solutions. To validate our findings, we compare them with numerical results obtained using the element–free Galerkin method. The comparison confirms the consistency and accuracy of the asymptotic approach.

**Keywords:** integrable potential; spectral parameter; boundary value problems; asymptotic estimates
**Mathematics Subject Classification:** 34B09, 34B30, 34L15

## 1. Introduction

In recent years, interest has been opened at the dependent spectral parameter in the boundary conditions for ordinary differential equations. We allow for one of these problems as follows:

$$u''(x) + \{\lambda - v(x)\} u(x) = 0, \quad x \in [0,1], \tag{1.1}$$

$$\left[\alpha_0 + \alpha_1 \lambda^{1/2} + \alpha_2 \lambda\right] u(0) + u'(0) = 0, \tag{1.2}$$

$$\left[\beta_0 + \beta_1 \lambda^{1/2} + \beta_2 \lambda\right] u(1) + u'(1) = 0. \tag{1.3}$$

Here, $\lambda$ is a spectral parameter; potential function $v(x)$ is real-valued and integrable on the related interval; $\alpha_i$ and $\beta_i$, $i = 0, 1, 2$ are real constants.

Equation (1.1) is usually derived from partial differential equations. For example, suppose that the specific heat $c(x)$, density $\rho(x)$ and thermal conductivity $K_0(x)$ (all depend on the spatial variable $x$)

that the heat source $Q(x,t) = \alpha(x)u(x,t)$ satisfies Newton's Law of Cooling, which is proportional to heat in the bar (with environmental temperature being zero). This gives the Heat Equation

$$c\rho\frac{\partial u}{\partial t} = \frac{\partial}{\partial x}\left[K_0\frac{\partial u}{\partial x}\right] + \alpha u.$$

Apply separation of variables, $u(x,t) = \phi(x)h(t)$, to the PDE and rearrange to

$$\frac{h'}{h} = \frac{1}{c\rho\phi}\frac{d}{dx}\left[K_0\frac{d\phi}{dx}\right] + \frac{\alpha}{c\rho} = -\lambda.$$

The differential equation in $x$ is

$$\frac{d}{dx}\left[K_0\frac{d\phi}{dx}\right] + \alpha\phi + c\rho\lambda\phi = 0.$$

This heat equation is a Sturm–Liouville equation and can be easily expressed as (1.1), and we note that different conditions with this equation give different problem formulations. Many authors have studied Sturm–Liouville equations with various boundary conditions. Some examples of recent work include [15, 16]. A special case of the Sturm–Liouville boundary value problem is considered in [15]. It calls the modified second Paine–de Hoog–Anderssen problem and estimates the lowest-order eigenvalue without solving the eigenvalue problem but by utilizing the localized landscape and effective potential functions instead. The transformation of the Sturm–Liouville problem from its canonical form to the Schrödinger form and its inverse are discussed in [16]. This study also focuses on the second Paine–de Hoog–Anderssen problem, which generalizes the corresponding invariant function to include arbitrary positive constants while maintaining its reciprocal quadratic power, and while an exact canonical form is not possible to obtain, it successfully derives the Sturm–Liouville problem in its canonical form asymptotically.

In this paper, we study symmetric potential. Especially in recent years, since quantum mechanic has gained importance, there have been a lot of studies on eigenvalues of Hill' s equation and the Schrödinger operator with symmetric potential. For example, in a symmetric hydrogen bond that occurs in many biological structures such as DNA and water, the proton free energy landscape is a symmetric single potential. The unusual case of very strong H-bonds features symmetric single-well proton free energy profiles; in this particular case the energy minimum corresponds to the proton centered in the middle of the H-bond, and therefore no PT transfer barrier exists. This conclusion is reached in [21]. The analytical and numerical results for nonharmonic, undamped, single-well, stochastic oscillators driven by additive noises are discussed in [20]. It also focuses on average kinetic, potential, and total energies together with the corresponding distributions under random drivings, involving Gaussian white, Ornstein-Uhlenbeck, and Markovian dichotomous noises. The inverse nodal problem and the eigenvalue gap for the one-dimensional sloshing problem with the p-Laplacian operator are studied in [5]. They also investigate the eigenvalue gap under the restriction of symmetric single-well depth functions. The analytical transfer matrix method to solve the energy splitting in an arbitrary symmetric double well potential is extended in [23]. The semiclassical periodic orbit theory is applied to the double-well eigenvalue problem to show how the unified approach describes the quite different character of the level splitting (in the case of symmetric wells) and level shifts (in the asymmetric case) caused by tunneling in [22].

The problems that are similar to (1.1)–(1.3) have eigenparameters in the boundary conditions and are encountered in physics and engineering problems. These applied problems are given in [8, 9].

The problems that have eigenparameters in the boundary conditions, like (1.1)–(1.3), are studied in [1, 2, 12–14]. We especially refer to [17]. This study considers (1.1)–(1.3) for nonnegative continuous potential, and they obtain asymptotic estimates for eigenvalues and eigenfunctions. It proves that when the conditions for $\alpha_i$ and $\beta_i$

$$\alpha_0 < 0, \alpha_2 > 0, \beta_0 > 0, \beta_2 < 0, |\alpha_1| + |\beta_1| \neq 0 \tag{1.4}$$

are satisfied, the following properties exist:

- The eigenvalues of the boundary value problems (1.1)–(1.3) are real.
- The eigenvalues of the boundary value problems (1.1)–(1.3) constitute an at most countable set without finite limit points. All eigenvalues of the boundary value problemS (1.1)–(1.3) are simple.
- The number $\lambda = 0$ is not an eigenvalue of the boundary value problems (1.1)–(1.3).
- There are an unboundedly decreasing sequence of negative eigenvalues $(\lambda_{-n}^{1/2})$ and an unboundedly increasing sequence of positive eigenvalues $(\lambda_n^{1/2})$ of the boundary value problems (1.1)–(1.3).

In this study, our aim is to determine the eigenvalue of (1.1)–(1.3). Firstly, in Section 2, we introduce our asymptotic method to calculate eigenvalues. In Section 3, we approximate eigenvalues for integrable potential under the condition (1.4) in Theorem 3.1, and then we present our solutions for symmetric potential in the Corollary 3.1. We especially deal with symmetric situations, because the symmetric potential is an important function, especially in quantum mechanics, and frequently used in inverse Sturm–Liouville problems. And hence, our analysis confirmed that a symmetric potential allows us to consider only half of the range. We don't need to study the entire interval for symmetric potential. After calculating asymptotic eigenvalues of (1.1)–(1.3), in Section 4, the element–free Galerkin (EFG) method [3], which is used for the comparison of asymptotic solutions, is discussed. This method, which is one of the meshless methods, obtains shape functions using the moving least squares (MLS) approach [18]. Utilizing the weak form of the problem, this numerical method applies to a wide range of problems [6, 19, 24]. To solve the waveguide eigenvalue problem, the interpolating element–free Galerkin scaled boundary method is used by [4]. Also, a combination of the numerical mode-matching (NMM) method and the EFG method is employed by [7] to address electromagnetic wave problems in cylindrically layered structures with multiple horizontal layers. In the EFG scheme, they obtain the matrix form of the generalized eigenvalue equation. And finally, in Section 5, we exemplify our results for different potentials.

## 2. Asymptotic method

At the beginning, we point out that just for the sake of simplicity, we accept $\int_0^1 v(x)\,dx = 0$ as in [10]. The condition is clearly not a restriction on $v(x)$. If $v(x)$ has a nonzero mean value, say $c$, we work on the following equation:

$$u''(x) + \{(\lambda - c) - (v(x) - c)\}\, u(x) = 0,$$

in which $v(x) - c$ has a mean value of zero.

We apply the transformation $U(x, \lambda) := \dfrac{u'(x, \lambda)}{u(x, \lambda)}$ to (1.1) and we find the following Riccati equation for (1.1):

$$U'(x,\lambda) = -\lambda + v(x) - U^2(x,\lambda).$$

Let us indicate the real and imaginary part of $U(x,\lambda)$ as

$$S(x,\lambda) := Re[U(x,\lambda)], \tag{2.1}$$

$$T(x,\lambda) := Im[U(x,\lambda)]. \tag{2.2}$$

We see in [11] that

$$u(x,\lambda) = R(x,\lambda)\cos\theta(x,\lambda) \tag{2.3}$$

so that

$$S(x,\lambda) = \frac{R'(x,\lambda)}{R(x,\lambda)}, \tag{2.4}$$

and

$$T(x,\lambda) = \theta'(x,\lambda). \tag{2.5}$$

Here $u(x,\lambda)$ is a real-valued solution of (1.1). By integrating the both sides of (2.5) from 0 to 1, we find that

$$\theta(1,\lambda) - \theta(0,\lambda) = \int_0^1 T(x,\lambda)\,dx. \tag{2.6}$$

We use the last equality to compute asymptotic approximations for the eigenvalues of (1.1)–(1.3).

Our estimating method based on the solution of $U'(x,\lambda) = -\lambda + v - U^2$ on $[0,1]$ is similar to [11], so we suppose that there exist functions $A(t)$ and $\eta(\lambda)$ so that

$$\left|\int_t^1 e^{2i\lambda^{1/2}x} v(x)\,dx\right| \le A(t)\,\eta(\lambda), \quad t \in [0,1]$$

where i) $A(t) := \int_t^1 |v(x)|\,dx$ is a decreasing function of $t$,

ii) $A(t) \in L[0,1]$,

iii) $\eta(\lambda) \to 0$ as $\lambda \to \infty$.

For $v \in L[0,1]$, the existence of the functions $A$ and $\eta$ may be established for $\lambda$ positive as follows. It is clear that $\left|\int_t^1 e^{2i\lambda^{1/2}x} v(x)\,dx\right| \le \int_t^1 |v(x)|\,dx < \infty$, hence, if we define

$$F(t,\lambda) := \begin{cases} \left|\int_t^1 e^{2i\lambda^{1/2}x} v(x)\,dx\right| / \int_t^1 |v(x)|\,dx, & \text{if } \int_t^1 |v(x)|\,dx \neq 0, \\ 0 \qquad\qquad\qquad\qquad\qquad\quad , & \text{if } \int_t^1 |v(x)|\,dx = 0, \end{cases} \tag{2.7}$$

we gain $0 \le F(t,\lambda) \le 1$. Also, if we set $\eta(\lambda) := \sup_{a\le t\le b} F(t,\lambda)$, we have $\eta(\lambda)$ is well defined by Eq (2.7) and $\eta(\lambda) \to 0$ as $\lambda \to \infty$ [11].

Similar to [10], let us set

$$U(x,\lambda) := i\lambda^{1/2} + \sum_{n=1}^{\infty} U_n(x,\lambda). \tag{2.8}$$

By using the last equation in Riccati equation and solving that differential equation, we gain

$$U_1(x,\lambda) = -e^{-2i\lambda^{1/2}x} \int_x^1 v(t)\,e^{2i\lambda^{1/2}t} dt,$$

$$U_2(x,\lambda) = e^{-2i\lambda^{1/2}x}\int_x^1 U_1^2(t,\lambda)\, e^{2i\lambda^{1/2}t}dt, \tag{2.9}$$

$$U_n(x,\lambda) = e^{-2i\lambda^{1/2}x}\int_x^1 [\ U_{n-1}^2(t,\lambda) + 2U_{n-1}(t,\lambda)\sum_{m=1}^{n-2} U_m(t,\lambda)\ ]\, e^{2i\lambda^{1/2}t}dt, \quad n \geq 3.$$

Substitution of (2.2) and (2.8) into (2.6) shows $\theta(1,\lambda) - \theta(0,\lambda) = \int_0^1 \left[\lambda^{1/2} + Im\sum_{n=1}^{\infty} U_n(t,\lambda)\right]dt$, and then

$$\theta(1,\lambda) - \theta(0,\lambda) = \lambda^{1/2} + \sum_{n=1}^{\infty} Im\int_0^1 U_n(t,\lambda)\,dt. \tag{2.10}$$

As a result of $|U_n(x,\lambda)| \leq k_n\eta(\lambda)^n$ in [11], we have as $\lambda \to \infty$

$$U(x,\lambda) = i\lambda^{1/2} + U_1(x,\lambda) + O\left(\eta^2(\lambda)\right) \tag{2.11}$$

where

$$\begin{aligned} U_1(x,\lambda) &= -e^{-2i\lambda^{1/2}x}\int_x^1 e^{2i\lambda^{1/2}t}v(t)\,dt \\ &= -\left[\cos 2\lambda^{1/2}x - i\sin 2\lambda^{1/2}x\right]\int_x^1 \left[\cos 2\lambda^{1/2}t + i\sin 2\lambda^{1/2}t\right]v(t)\,dt. \end{aligned} \tag{2.12}$$

Hence, by using (2.11) and (2.12) in (2.1), we have

$$S(x,\lambda) = -\left(\cos 2\lambda^{1/2}x\right)\int_x^1 v(t)\left[\cos 2\lambda^{1/2}t\right]dt - \left(\sin 2\lambda^{1/2}x\right)\int_x^1 v(t)\left[\sin 2\lambda^{1/2}t\right]dt + O\left(\eta^2(\lambda)\right).$$

Let us define the following notations for abbreviation:

$$\begin{aligned} \sin\xi_x &:= \int_x^1 v(t)\left[\cos 2\lambda^{1/2}t\right]dt, \\ \cos\xi_x &:= \int_x^1 v(t)\left[\sin 2\lambda^{1/2}t\right]dt. \end{aligned}$$

Thus, we can write $S(t,\lambda)$ as

$$S(x,\lambda) = -\sin\left(2\lambda^{1/2}x + \xi_x\right) + O\left(\eta^2(\lambda)\right). \tag{2.13}$$

Similarly, by using (2.11) and (2.12) in (2.2), $T(x,\lambda)$ is presented as

$$T(x,\lambda) = \lambda^{1/2} - \cos\left(2\lambda^{1/2}x + \xi_x\right) + O\left(\eta^2(\lambda)\right). \tag{2.14}$$

By using integration by parts on $U_1(x,\lambda)$ in (2.9), we hold that

$$\int_0^1 U_1(t,\lambda)\,dt = \frac{i}{2\lambda^{1/2}}\int_0^1 v(t)\, e^{2i\lambda^{1/2}t}dt$$

$$= \frac{i}{2}\lambda^{-1/2}\int_0^1 v(t)\left[\cos 2\lambda^{1/2}t\right]dt + \frac{i}{2}\lambda^{-1/2}\int_0^1 iv(t)\left[\sin 2\lambda^{1/2}t\right]dt,$$

and so

$$Im\int_0^1 U_1(t,\lambda)\,dt = \frac{1}{2}\lambda^{-1/2}\int_0^1 v(t)\left[\cos 2\lambda^{1/2}t\right]dt.$$

Here, we use $\int_0^1 v(x)\,dx = 0$. We also calculate from Eq (2.9) by using integration by part as

$$\int_0^1 U_2(t,\lambda)\,dt = \frac{i}{2\lambda^{1/2}}\int_0^1 U_1^2(t,\lambda)\left[1-e^{2i\lambda^{1/2}t}\right]dt$$

and for $n \geq 3$

$$\int_0^1 U_n(t,\lambda)\,dt = \frac{i}{2\lambda^{1/2}}\int_0^1 \left[1-e^{2i\lambda^{1/2}t}\right]\times\left[U_{n-1}^2(t,\lambda) + 2U_{n-1}(t,\lambda)\sum_{m=1}^{n-2}U_m(t,\lambda)\right]dt.$$

Thus, with the last equations, we have the following estimate:

$$\begin{aligned}\int_0^1 \sum_{n=1}^{\infty} Im\{U_n(t,\lambda)\}\,dt &= \sum_{n=1}^{\infty} Im\left\{\int_0^1 U_n(t,\lambda)\,dt\right\}\\ &= \frac{1}{2}\lambda^{-1/2}\int_0^1 v(t)\left[\cos 2\lambda^{1/2}t\right]dt + O\left(\lambda^{-1}\eta(\lambda)\right). \qquad (2.15)\end{aligned}$$

## 3. Results

In this paper, we demonstrate these conclusions:

**Theorem 3.1.** *As $n \to \infty$, the eigenvalues of the problems (1.1)–(1.3) satisfy*

$$\begin{aligned}\lambda_n^{1/2} &= (n+1)\pi - \frac{1}{(n+1)\pi}\left\{\frac{1}{\beta_2} - \frac{1}{\alpha_2} + \frac{1}{2}\int_0^1 v(t)\left[\cos 2(n+1)\pi t\right]dt\right\}\\ &+ \frac{1}{(n+1)^2\pi^2}\left\{\frac{\beta_1}{(\beta_2)^2} - \frac{\alpha_1}{(\alpha_2)^2} - \frac{1}{\alpha_2}\int_0^1 v(t)\left[\sin 2(n+1)\pi t\right]dt\right\} + O\left(n^{-2}\eta(n)\right).\end{aligned}$$

*Proof.* Firstly, let us compute the derivative of $U(x,\lambda)$ from (2.3):

$$U'(x,\lambda) = R'(x,\lambda)\cos\theta(x,\lambda) - R(x,\lambda)\theta'(x,\lambda)\sin\theta(x,\lambda). \qquad (3.1)$$

By using the last equation and (2.3) in (1.2), we obtain

$$R(0,\lambda)\left\{\left[\alpha_0 + \alpha_1\lambda^{1/2} + \alpha_2\lambda + \frac{R'(0,\lambda)}{R(0,\lambda)}\right]\cos\theta(0,\lambda) - \theta'(0,\lambda)\sin\theta(0,\lambda)\right\} = 0.$$

If we choose $\gamma_1$ as

$$\sin\gamma_1 := \alpha_0 + \alpha_1\lambda^{1/2} + \alpha_2\lambda + \frac{R'(0,\lambda)}{R(0,\lambda)},$$

$$\cos\gamma_1 := \theta'(0,\lambda),$$

we collect $R(0,\lambda)\sin[\gamma_1 - \theta(0,\lambda)] = 0$, so $\sin(\gamma_1 - \theta(0,\lambda)) = 0$, i.e., $\theta(0,\lambda) = \gamma_1$.

Using by substitutions of $S(x,\lambda) = \frac{R'(x,\lambda)}{R(x,\lambda)}$, $T(x,\lambda) = \theta'(x,\lambda)$ as in (2.4), (2.5), and their asymptotic expansions (2.13) and (2.14) into the definitions of $\sin\gamma_1$ and $\sin\gamma_2$, we obtain

$$\frac{\cos\gamma_1}{\sin\gamma_1} = \frac{\lambda^{1/2} - \cos(\xi_0) + O\left(\eta^2(\lambda)\right)}{\alpha_0 + \alpha_1\lambda^{1/2} + \alpha_2\lambda - \sin(\xi_0) + O(\eta^2(\lambda))},$$

hence

$$\frac{\cos\gamma_1}{\sin\gamma_1} = \frac{\lambda^{1/2} - \cos(\xi_0) + O\left(\eta^2(\lambda)\right)}{\alpha_2\lambda\left[1 + \frac{\alpha_1}{\alpha_2}\lambda^{-1/2} + \frac{\alpha_0}{\alpha_2}\lambda^{-1} - \frac{\sin(\xi_0)}{\alpha_2}\lambda^{-1} + O(\lambda^{-1}\eta^2(\lambda))\right]}.$$

Because of $\sum_{n=0}^{\infty}(-1)^n x^n = \frac{1}{1+x}$, then

$$\begin{aligned}\cot\gamma_1 = &\left[\frac{1}{\alpha_2}\lambda^{-1/2} - \frac{\cos(\xi_0)}{\alpha_2}\lambda^{-1} + O\left(\lambda^{-1}\eta^2(\lambda)\right)\right]\\ &\times\left[1 - \frac{\alpha_1}{\alpha_2}\lambda^{-1/2} - \frac{\alpha_0}{\alpha_2}\lambda^{-1} + \frac{\sin(\xi_0)}{\alpha_2}\lambda^{-1} + \left(\frac{\alpha_1}{\alpha_2}\right)^2\lambda^{-1} + O\left(\lambda^{-1}\eta^2(\lambda)\right)\right]\end{aligned}$$

and so

$$\cot\gamma_1 = \frac{1}{\alpha_2}\lambda^{-1/2} - \frac{\cos(\xi_0)}{\alpha_2}\lambda^{-1} - \frac{\alpha_1}{(\alpha_2)^2}\lambda^{-1} + O\left(\lambda^{-1}\eta^2(\lambda)\right).$$

If we apply inverse cotangent expansion formula $\cot^{-1}(\delta) = \frac{\pi}{2} - \delta + \frac{\delta^3}{3} + ...$ to the last equation, we calculate $\gamma_1$ as follows:

$$\gamma_1 = \frac{\pi}{2} - \frac{1}{\alpha_2}\lambda^{-1/2} + \frac{\cos(\xi_0)}{\alpha_2}\lambda^{-1} + \frac{\alpha_1}{(\alpha_2)^2}\lambda^{-1} + O\left(\lambda^{-1}\eta^2(\lambda)\right). \tag{3.2}$$

In similar manner, when we use the form $U(x,\lambda) = R(x,\lambda)\cos\theta(x,\lambda)$ for boundary $x = 1$, with (3.1), we obtain

$$R(1,\lambda)\left\{\left[\beta_0 + \beta_1\lambda^{1/2} + \beta_2\lambda + \frac{R'(1,\lambda)}{R(1,\lambda)}\right]\cos\theta(1,\lambda) - \theta'(1,\lambda)\sin\theta(1,\lambda)\right\} = 0.$$

From the last equation, if we choose $\gamma_2$ as

$$\begin{aligned}\sin\gamma_2 &:= \alpha_0 + \alpha_1\lambda^{1/2} + \alpha_2\lambda + \frac{R'(1,\lambda)}{R(1,\lambda)},\\ \cos\gamma_2 &:= \theta'(1,\lambda),\end{aligned}$$

we access that $R(1,\lambda)\sin[\gamma_2 - \theta(1,\lambda)] = 0$, so $\sin(\gamma_2 - \theta(1,\lambda)) = 0$, i.e., $\theta(1,\lambda) = \gamma_2 + (n+1)\pi$. By substitution of (2.4) and (2.5) for boundary $x = 1$ and using their asymptotic estimates (2.13) and (2.14), we catch the following:

$$\frac{\cos\gamma_2}{\sin\gamma_2} = \frac{\lambda^{1/2} - \cos(\xi_1) + O\left(\eta^2(\lambda)\right)}{\beta_0 + \beta_1\lambda^{1/2} + \beta_2\lambda - \sin(\xi_1) + O(\eta^2(\lambda))}.$$

From the definition of $\xi_x$, since $\cos(\xi_1) = \sin(\xi_1) = 0$, we hold from the last equation:

$$\frac{\cos\gamma_2}{\sin\gamma_2} = \frac{\lambda^{1/2} + O\left(\eta^2(\lambda)\right)}{\beta_2\lambda\left[1 + \frac{\beta_1}{\beta_2}\lambda^{-1/2} + \frac{\beta_0}{\beta_2}\lambda^{-1} + O\left(\lambda^{-1}\eta^2(\lambda)\right)\right]}.$$

Because of

$$\sum_{n=0}^{\infty}(-1)^n x^n = \frac{1}{1+x},$$

we have

$$\cot\gamma_2 = \left[\frac{1}{\beta_2}\lambda^{-1/2} + O\left(\lambda^{-1}\eta^2(\lambda)\right)\right] \times \left[1 - \frac{\beta_1}{\beta_2}\lambda^{-1/2} - \frac{\beta_0}{\beta_2}\lambda^{-1} + \left(\frac{\beta_1}{\beta_2}\right)^2\lambda^{-1} + O\left(\lambda^{-1}\eta^2(\lambda)\right)\right],$$

and so

$$\cot\gamma_2 = \frac{1}{\beta_2}\lambda^{-1/2} - \frac{\beta_1}{(\beta_2)^2}\lambda^{-1} + O\left(\lambda^{-1}\eta^2(\lambda)\right).$$

In the last equation, by using inverse cotangent expansion formula

$$\cot^{-1}(\delta) = \frac{\pi}{2} - \delta + \frac{\delta^3}{3} + ...,$$

we gain $\gamma_2$ as follows:

$$\gamma_2 = \frac{\pi}{2} - \frac{1}{\beta_2}\lambda^{-1/2} + \frac{\beta_1}{(\beta_2)^2}\lambda^{-1} + O\left(\lambda^{-1}\eta^2(\lambda)\right). \tag{3.3}$$

Let us use these findings (2.15), (3.2) and (3.3) in

$$\theta(1,\lambda) - \theta(0,\lambda) = \lambda^{1/2} + \sum_{n=1}^{\infty} Im\int_0^1 U_n(t,\lambda)\,dt,$$

(as in (2.10)), we view that

$$\begin{aligned}(n+1)\pi + \frac{\pi}{2} - \frac{1}{\beta_2}\lambda^{-1/2} + \frac{\beta_1}{(\beta_2)^2}\lambda^{-1} - \frac{\pi}{2} + \frac{1}{\alpha_2}\lambda^{-1/2} - \frac{\cos(\xi_0)}{\alpha_2}\lambda^{-1} - \frac{\alpha_1}{(\alpha_2)^2}\lambda^{-1} \\ + O\left(\lambda^{-1}\eta^2(\lambda)\right) = \lambda^{1/2} + \frac{1}{2}\lambda^{-1/2}\int_0^1 v(t)\left[\cos 2\lambda^{1/2}t\right]dt + O\left(\lambda^{-1}\eta(\lambda)\right).\end{aligned}$$

By using definitions of $\cos\xi_x, \eta(\lambda)$ and reversion in the last equation, we prove the theorem. □

**Corollary 3.1.** *As $n \to \infty$, the eigenvalues of the problems (1.1)–(1.3) with symmetric potential satisfy*

$$\begin{aligned}\lambda_n^{1/2} = (n+1)\pi - \frac{1}{(n+1)\pi}\left\{\frac{1}{\beta_2} - \frac{1}{\alpha_2} + \int_0^{1/2} v(t)\left[\cos 2(n+1)\pi t\right]dt\right\} \\ + \frac{1}{(n+1)^2\pi^2}\left\{\frac{\beta_1}{(\beta_2)^2} - \frac{\alpha_1}{(\alpha_2)^2}\right\} + O\left(n^{-2}\eta(n)\right).\end{aligned}$$

*Proof.* To prove the corollary, let us calculate the following integral by using symmetric potential, i.e., $v(x) = v(1-x)$:

$$\begin{aligned}\int_{1/2}^{1} v(t)\left[\cos 2(n+1)\pi t\right]dt &= \int_{1/2}^{1} v(1-t)\left[\cos 2(n+1)\pi t\right]dt \\ &= -\int_{1/2}^{0} v(u)\left[\cos 2(n+1)\pi(1-u)\right]du \\ &= \int_{0}^{1/2} v(u)\left[\cos\left\{2(n+1)\pi - 2(n+1)\pi u\right\}\right]du \\ &= \int_{0}^{1/2} v(t)\left[\cos 2(n+1)\pi t\right]dt \end{aligned} \tag{3.4}$$

and similarly,

$$\begin{aligned}\int_{1/2}^{1} v(t)\left[\sin 2(n+1)\pi t\right]dt &= \int_{1/2}^{1} v(1-t)\left[\sin 2(n+1)\pi t\right]dt \\ &= -\int_{1/2}^{0} v(u)\left[\sin 2(n+1)\pi(1-u)\right]du \\ &= -\int_{0}^{1/2} v(t)\left[\sin 2(n+1)\pi t\right]dt. \end{aligned} \tag{3.5}$$

Hence, by using (3.4) and (3.5), we hold that

$$\begin{aligned}\int_{0}^{1} v(t)\left[\cos 2(n+1)\pi t\right]dt &= \int_{0}^{1/2} v(t)\left[\cos 2(n+1)\pi t\right]dt + \int_{1/2}^{1} v(t)\left[\cos 2(n+1)\pi t\right]dt \\ &= 2\int_{0}^{1/2} v(t)\left[\cos 2(n+1)\pi t\right]dt \end{aligned}$$

and

$$\begin{aligned}\int_{0}^{1} v(t)\left[\sin 2(n+1)\pi t\right]dt &= \int_{0}^{1/2} v(t)\left[\sin 2(n+1)\pi t\right]dt \\ &\quad + \int_{1/2}^{1} v(t)\left[\sin 2(n+1)\pi t\right]dt = 0. \end{aligned}$$

Substitution of the last two equations into Theorem 3.1 proves the corollary. □

## 4. Numerical method

### *4.1. The moving least square (MLS) method*

In this section, the EFG method, which is used to compare the results obtained in the previous section, is introduced. In this method, shape functions are constructed by using the MLS approach. Furthermore, the weak form of the problem is employed to obtain the numerical solution.

The local approximation function is given as

$$u^h(x,\overline{x}) = \sum_{i=1}^{m} p_i(x)a_i(\overline{x}) = \mathbf{p}^T(x)\mathbf{a}(\overline{x}). \tag{4.1}$$

Here, $p_i(x), a_i(\overline{x}), i = 1,2,...,m$, denote the monomial basis functions, and the unknown functions, respectively. $m$ is the number of basis functions, and $\overline{x}$ is a point in the domain of influence of $x$ where the shape function takes nonzero values.

The weighted discrete $L_2$ norm is defined as

$$\|f\|_w^2 = \sum_{i=1}^{N} w(\overline{x} - x_i)[f(x_i)]^2.$$

Here, $x_i, w(\overline{x} - x_i), i = 1,2,...,N$ are the nodal points and the weight functions centered at $x_i$, respectively. Also, $N$ is the number of nodal points. In the MLS method, the unknown functions in (4.1) are calculated by minimizing

$$J = \left\|u^h(x,\overline{x}) - U\right\|_w^2 = \sum_{i=1}^{N} w(\overline{x} - x_i)[u^h(x_i,\overline{x}) - u_i]^2.$$

Here, $u_i, i = 1,2,...,N$ are the node parameters at $x = x_i$. So, from $\frac{\partial J}{\partial \mathbf{a}} = 0$, it is obtained the system

$$A(\overline{x})\mathbf{a}(\overline{x}) = B(\overline{x})\mathbf{U}. \tag{4.2}$$

Here,

$$A(\overline{x}) = \sum_{i=1}^{N} w(\overline{x} - x_i)\mathbf{p}(x_i)\mathbf{p}^T(x_i),$$

$$B(\overline{x}) = \left[\begin{array}{cccc} w(\overline{x} - x_1)\mathbf{p}(x_1) & w(\overline{x} - x_2)\mathbf{p}(x_2) & \cdots & w(\overline{x} - x_N)\mathbf{p}(x_N) \end{array}\right],$$

$$\mathbf{U} = \left[\begin{array}{cccc} u_1 & u_2 & \cdots & u_N \end{array}\right]^T.$$

From (4.2), the unknown vector in (4.1) is calculated as

$$\mathbf{a}(\overline{x}) = A^{-1}(\overline{x})B(\overline{x})\mathbf{U}.$$

So, the local approximation function is obtained as

$$u^h(x,\overline{x}) = \mathbf{p}^T(x)A^{-1}(\overline{x})B(\overline{x})\mathbf{U}.$$

From here, the global approximation is given as

$$u^h(x) = \mathbf{p}^T(x)A^{-1}(x)B(x)\mathbf{U}. \tag{4.3}$$

If it is defined by

$$\Phi(x) := \mathbf{p}^T(x)A^{-1}(x)B(x)$$

in (4.3), the global approximation is found as

$$u^h(x) = \Phi(x)\mathbf{U} = \sum_{i=1}^{N} \phi_i(x)u_i. \tag{4.4}$$

The functions $\phi_i(x), i = 1, 2, ..., N$ in (4.4) are called shape functions centered at $x_i$. In this study, the cubic spline functions are chosen as the weight functions:

$$w(x - x_i) \equiv w(r) = \begin{cases} \frac{2}{3} - 4r^2 + 4r^3, & r \le \frac{1}{2} \\ \frac{4}{3} - 4r + 4r^2 - \frac{4}{3}r^3, & \frac{1}{2} < r \le 1. \\ 0, & r > 1 \end{cases}$$

Here, $r = \frac{\|x-x_i\|}{d_{mi}}$ is called the normalized radius function. $d_{mi}$ is a parameter that must be chosen to ensure the existence of the matrix $A^{-1}$.

The nodes $0, 0.2, 0.4, 0.6, 0.8$, and $1$ in the interval $[0, 1]$ are selected to illustrate the behavior of the shape functions. By choosing $d_{mi} = 0.3$, the shape functions at each node are obtained as illustrated in Figure 1.

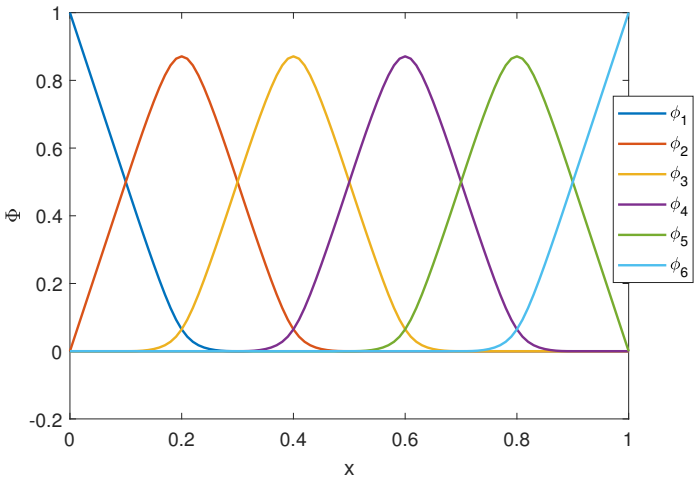


**Figure 1.** MLS shape functions for $d_{mi} = 0.3$ and nodes located at $0, 0.2, 0.4, 0.6, 0.8$, and $1$

Figure 1 demonstrates that each shape function attains its maximum value at its corresponding node. Each shape function $\phi_i$, $i = 1, 2, \ldots, 6$, is nonzero only within the interval $(x_i - d_{mi}, x_i + d_{mi})$ and vanishes outside this range. This interval is called the influence domain of the $i$th shape function.

### *4.2. Element–free Galerkin (EFG) scheme*

The EFG method is a type of meshless method commonly employed for solving differential equations or determining the eigenvalues of Sturm–Liouville problems. In this method, the weak form of the problem is generally used. To obtain the weak form, the problem (1.1) is multiplied by test function $\mu(x)$ and integrated over the problem domain

$$\int_0^1 u''(x)\mu(x)dx + \int_0^1 \{\lambda - v(x)\}\, u(x)\mu(x)dx = 0. \tag{4.5}$$

If integration by parts is applied to the first terms in the (4.5), we have

$$u'(x)\mu(x)|_{x=0}^{x=1} - \int_0^1 u'(x)\mu'(x)dx + \int_0^1 \{\lambda - v(x)\}\, u(x)\mu(x)dx = 0.$$

With boundary conditions in (1.2) and (1.3), the weak form is obtained as

$$\begin{aligned}&(\alpha_0 + \alpha_1\lambda^{1/2} + \alpha_2\lambda)u(0)\mu(0) - (\beta_0 + \beta_1\lambda^{1/2} + \beta_2\lambda)u(1)\mu(1) \\ &- \int_0^1 u'(x)\mu'(x)dx + \int_0^1 \{\lambda - v(x)\}\, u(x)\mu(x)dx = 0.\end{aligned} \tag{4.6}$$

By substituting the approximation in (4.4) into the weak form in (4.6) and selecting the shape functions as test functions, the system equation is obtained as

$$\begin{aligned}&\sum_{i=1}^{N}\left[(\alpha_0 + \alpha_1\lambda^{1/2} + \alpha_2\lambda)\phi_i(0)\phi_j(0) - (\beta_0 + \beta_1\lambda^{1/2} + \beta_2\lambda)\phi_i(1)\phi_j(1)\right]U_i \\ &+ \sum_{i=1}^{N}\left[\int_0^1 (\lambda - v(x))\,\phi_i(x)\phi_j(x)dx - \int_0^1 \frac{d\phi_i(x)}{dx}\frac{d\phi_j(x)}{dx}dx\right]U_i = 0,\ j = 1, 2, ..., N.\end{aligned} \tag{4.7}$$

When we use the following definitions

$$(B_1)_{i,j} := \phi_i(0)\phi_j(0), (B_2)_{i,j} := \phi_i(1)\phi_j(1), M_{i,j} := \int_0^1 \frac{d\phi_i(x)}{dx}\frac{d\phi_j(x)}{dx}dx$$

$$K_{i,j} := \int_0^1 \phi_i(x)\phi_j(x)dx, C_{i,j} := \int_0^1 v(x)\phi_i(x)\phi_j(x)dx, 1 \le i, j \le N,$$

in (4.7), the system equation is found as

$$\left[(\alpha_0 + \alpha_1\lambda^{1/2} + \alpha_2\lambda)B_1 - (\beta_0 + \beta_1\lambda^{1/2} + \beta_2\lambda)B_2 - M + \lambda K - C\right]U = 0.$$

So, the numerical eigenvalues in (1.1) are obtained by finding the roots of the characteristic equation

$$F(\lambda) = \det\left((\alpha_0 + \alpha_1\lambda^{1/2} + \alpha_2\lambda)B_1 - (\beta_0 + \beta_1\lambda^{1/2} + \beta_2\lambda)B_2 - M + \lambda K - C\right). \tag{4.8}$$

The Newton-Raphson method can be employed to determine the roots of the function given in (4.8). This iterative method starts with an initial guess near the desired root. At each iteration, the x-intercept of the tangent line to the function at the current point is computed and used as the next approximation. Accordingly, the sequence of approximations in the Newton-Raphson method is determined by the following expression:

$$\lambda_{n+1} = \lambda_n - \frac{F(\lambda_n)}{F'(\lambda_n)}.$$

This procedure is repeated until the condition $|\lambda_{n+1} - \lambda_n| < \epsilon$, where $\epsilon$ is a user-defined tolerance, is satisfied. The final value of $\lambda_{n+1}$ obtained through this process is considered the approximated root.

## 5. Examples

### 5.1. Example 1

Our first example is the basic symmetric function $v(x) = x(1-x)$ on the interval $[0, 1]$. By evaluating the integral expressions in the corollary with the parameter values $\alpha_0 = -2, \alpha_1 = 2, \alpha_2 = 1, \beta_0 = 2, \beta_1 = 1, \beta_2 = -1$, we calculate the asymptotic eigenvalues of the problem defined by (1.1)–(1.3) as

$$\lambda_n^{1/2} = (n+1)\pi - \frac{1}{(n+1)\pi}\left\{-2 + \frac{1}{(n+1)\pi} + \frac{1}{4(n+1)^2\pi^2}\right\} + O\left(n^{-2}\eta(n)\right).$$

We now determine the optimal value of the parameter $d_{mi}$ in the numerical solution of the problem defined by (1.1)–(1.3). The relative error for various values of $d_{mi}$ is examined. In this study, the error is defined as the relative error between the asymptotic eigenvalues (obtained in Section 3) and the numerical eigenvalues (obtained in Section 4) and is expressed as follows:

$$E = \frac{|\text{asymptotic eigenvalue} - \text{numerical eigenvalue}|}{\text{asymptotic eigenvalue}}. \tag{5.1}$$

In the literature, $d_{mi}$ is generally selected as $d_{max}h$ for uniformly distributed nodes. Here, $h$ is the distance between nodes, and $d_{max}$ is a user-defined parameter. For static problems, this parameter is typically chosen between 2 and 4. Table 1 presents the relative errors corresponding to different values of $d_{max}$, with $h = 0.01$:

**Table 1.** The relative errors for different $d_{max}$ values for $v(x) = x(1-x)$.

| $n$ | $d_{max} = 1.75$ | $d_{max} = 2$ | $d_{max} = 2.75$ | $d_{max} = 3$ |
|---|---|---|---|---|
| 1 | 0.00498 | 0.00498 | 0.00498 | 0.00498 |
| 2 | 0.00109 | 0.00109 | 0.00109 | 0.00109 |
| 3 | 0.00034 | 0.00036 | 0.00035 | 0.00035 |
| 4 | 0.00012 | 0.00015 | 0.00013 | 0.00013 |
| 5 | 0.00003 | 0.00007 | 0.00004 | 0.00004 |
| 6 | 0.00001 | 0.00004 | 0.0000002 | 0.0000009 |
| 7 | 0.00004 | 0.00002 | 0.00003 | 0.00003 |
| 8 | 0.00007 | 0.00001 | 0.00005 | 0.00005 |
| 9 | 0.00009 | 0.000008 | 0.00007 | 0.00007 |
| 10 | 0.00011 | 0.000004 | 0.00009 | 0.00009 |

As can be seen from Table 1, the error values are quite close to each other for most eigenvalues. For the 6th eigenvalue, the smallest error is observed when $d_{max} = 2.75$, while for the 9th and 10th eigenvalues, the minimum error occurs at $d_{max} = 2$. However, since the overall error values are relatively close, the value $d_{max} = 2$ is selected for this study.

The following Table 2 presents the asymptotic and numerical eigenvalues for $d_{max} = 2$. The last column of Table 2 shows the relative errors as defined in Eq (5.1), and the eigenvalues computed using the asymptotic method are in close agreement with those obtained through the element-free Galerkin method. Moreover, the last row of the following table indicates that the relative errors are very small. Therefore, for $v(x) = x(1-x)$, the asymptotic and numerical results are in good agreement.

**Table 2.** Eigenvalue comparison for the symmetric potential $v(x) = x(1 - x)$.

| $n$ | Asymptotic Appr. | EFG Appr. | Relative Error ($E$) |
|---|---|---|---|
| 1 | 43.23269 | 43.44821 | 0.004985 |
| 2 | 92.64886 | 92.75073 | 0.0010995 |
| 3 | 161.77466 | 161.83366 | 0.0003647 |
| 4 | 250.62593 | 250.66417 | 0.0001526 |
| 5 | 359.20891 | 359.23561 | 0.0000743 |
| 6 | 487.52653 | 487.54604 | 0.00004 |
| 7 | 635.58039 | 635.59501 | 0.000023 |
| 8 | 803.37142 | 803.38238 | 0.0000136 |
| 9 | 990.90019 | 990.90819 | 0.0000081 |
| 10 | 1198.16709 | 1198.17245 | 0.0000045 |
| 15 | 2530.58029 | 2530.57122 | 0.0000036 |
| 20 | 4356.46601 | 4356.43719 | 0.0000066 |
| 25 | 6675.82861 | 6675.81047 | 0.0000027 |

Figure 2 presents the relative errors, as defined in Eq (5.1), for the first 20 eigenvalues as follows:

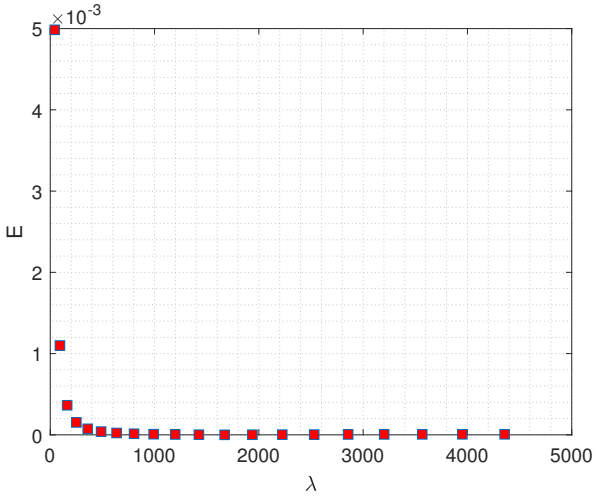


**Figure 2.** Relative errors ($E$) of the first 20 eigenvalues for $v(x) = x(1 - x)$.

As can be seen from Figure 2, the initial error values on the order of $10^{-3}$ decrease to nearly zero.

### *5.2. Example 2*

The second example is $v(x) = \cos(2x)$, and this function plays a significant role and appears in various forms as a potential in Schrödinger equations. It serves as a classical example of a symmetric double-well potential. Moreover, when we consider $v(x) = \epsilon \cos(2x)$ in Eq (1.1), the result is the well-known Mathieu Equation, where $\epsilon$ denotes a small, real-valued parameter. The Mathieu equation arises in a wide range of physical contexts—for instance, when solving the wave equation in elliptic coordinates. It also models motion in periodic potentials, such as the path of an electron through a lattice of atoms, the dynamics of a quantum pendulum, and the behavior of charged particles within a quadrupole mass spectrometer.

Therefore, by applying our findings to the case $v(x) = \cos(2x)$ on the interval $[0, 1]$, and by evaluating the integral expressions in the corollary by taking $\alpha_0 = -1, \alpha_1 = 0, \alpha_2 = 2, \beta_0 = 1$, $\beta_1 = 1, \beta_2 = -1$, we derive the asymptotic behavior of the problem defined by (1.1)–(1.3) as

$$\lambda_n^{1/2} = (n+1)\pi - \frac{1}{(n+1)\pi}\left\{-\frac{3}{2} + \frac{1}{(n+1)\pi} + \frac{(-1)^n \sin 1}{2\left[(n+1)^2\pi^2 - 1\right]}\right\} + O\left(n^{-2}\eta(n)\right).$$

Table 3 presents the asymptotic and numerical eigenvalues for $d_{max} = 2$. The relative errors are also given in the last column of Table 3:

**Table 3.** Eigenvalue comparison for the symmetric potential $v(x) = \cos(2x)$

| $n$ | Asymptotic Appr. | EFG Appr. | Relative Error ($E$) |
|---|---|---|---|
| 1 | 42.22826 | 42.84783 | 0.0146719 |
| 2 | 91.62637 | 92.06461 | 0.0047829 |
| 3 | 160.7727 | 161.08811 | 0.0019618 |
| 4 | 249.6177 | 249.87736 | 0.0010402 |
| 5 | 358.20793 | 358.41871 | 0.0005884 |
| 6 | 486.52229 | 486.70636 | 0.0003783 |
| 7 | 634.57982 | 634.73753 | 0.0002485 |
| 8 | 802.36885 | 802.51063 | 0.0001767 |
| 9 | 989.89982 | 990.02473 | 0.0001261 |
| 10 | 1197.16536 | 1197.27922 | 0.0000951 |
| 15 | 2529.58014 | 2529.64628 | 0.0000261 |
| 20 | 4355.46554 | 4355.49475 | 0.0000067 |
| 25 | 6674.82855 | 6674.85675 | 0.0000042 |

As shown in Table 3, the asymptotic eigenvalues and numerical eigenvalues yield consistent results. In the last row of Table 3, the relative errors are of small magnitude.

In Figure 3, the relative errors corresponding to the first 20 eigenvalues for the function $v(x) = \cos(2x)$ are shown:

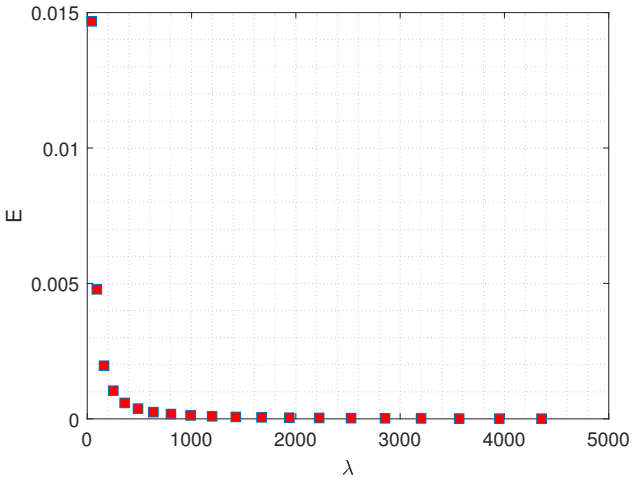


**Figure 3.** Relative errors ($E$) of the first 20 eigenvalues for $v(x) = \cos(2x)$.

Figure 3 demonstrates, similar to Example 1, that the errors gradually decrease and approach zero.

## 6. Conclusions

Firstly, the asymptotic expansion of the spectrum for a Sturm–Liouville problem with integrable potential is investigated in this study. These approximations for positive eigenvalues are obtained with better error terms than previous works in the literature. Also, we calculate our results for both integrable and symmetric potential because of the importance of symmetry, especially in quantum mechanics. It is very important that we prove if we have a symmetric potential, it is enough to study with the half interval. We don't need the whole interval.

Secondly, to ensure the reliability of asymptotic solutions, the eigenvalues of the problem are numerically calculated using the EFG method, which is one of the meshless methods. In this method, the shape functions are constructed via the MLS approach, and the weak form of the problem is generally used. Section 4 discusses the MLS method in detail and derives the weak form of problem (1.1). Subsequently, the system equation is formulated using the EFG method, and a function $F$ is obtained, whose roots correspond to the desired eigenvalues.

Two problems are analyzed to compare the asymptotic and numerical eigenvalues. In the first problem, it is observed that the optimal value of the $d_{max}$ parameter in the MLS method can be selected as 2. Then, the asymptotic and numerical eigenvalues are compared using this value. Examples 1 and 2 demonstrate that the relative error values are very small, indicating that the asymptotic results are both accurate and consistent. On the other hand, the use of machine learning to systematically select EFG shape function parameters (such as $d_{mi}$) has the potential to improve the overall comprehensiveness and extensibility of the method.

### Author contributions

All authors contributed equally to this work. All authors have accepted responsibility for the entire content of this manuscript and consented to its submission to the journal, reviewed all the results, and approved the final version of the manuscript.

### Use of Generative-AI tools declaration

The authors declare that they have not used Artificial Intelligence (AI) tools in the creation of this article.

### Acknowledgments

Both authors sincerely thank the referees for their insight and Recep Tayyip Erdoğan University for funding. This study has been supported by the Recep Tayyip Erdoğan University Development Foundation (Grant Number: 02025007001580).

### Conflict of interest

The authors declare no conflicts of interest.

## References


1. E. Başkaya, On the asymptotics of eigenvalues for a Sturm–Liouville problem with symmetric single-well potential, *Demonstr. Math.*, **57** (2024), 20230129. https://doi.org/10.1515/dema-2023-0129
2. E. Başkaya, On a boundary value problem with symmetric double well potential and spectral parameter in the boundary condition, *Sigma J. Eng. Nat. Sci.*, **42** (2024), 572–577. https://doi.org/10.14744/sigma.2024.00044
3. T. Belytscho, Y. Y. Lu, L. Gu, Element-free Galerkin methods, *Int. J. Numer. Methods Eng.*, **37** (1994), 229–256. https://doi.org/10.1002/nme.1620370205
4. S. Chen, H. Zhang, Q. Li, X. Wei, An interpolating element-free Galerkin scaled boundary method applied to waveguide eigenvalue problem, *Adv. Eng. Softw.,* **206** (2025), 103923. https://doi.org/10.1016/j.advengsoft.2025.103923
5. W. C. Chen, Y. Cheng, Remarks on the one-dimensional sloshing problem involving the p-Laplacian operator, *Turk. J. Math.*, **44** (2020), 1376–1387. https://doi.org/10.3906/mat-1908-90
6. H. Cui, Z. Meng, H. Cheng, L. Ma, The efficient element-free Galerkin method for 3D Schrödinger equations, *Int. J. Appl. Mech.*, **17** (2025), 2550022. https://doi.org/10.1142/S175882512550022X
7. Y. Dun, S. Zeng,, J. Chen, Element-free Galerkin numerical mode-matching method for static and time-harmonic electromagnetic fields in orthogonal-plano-cylindrically layered media, *Int. J. Numer. Model.: Electron. Netw. Devices Fields*, **34** (2021), e2837. https://doi.org/10.1002/jnm.2837
8. C. T. Fulton, Two point boundary value problems with eigenvalue parameter contained in the boundary conditions, *Proc. R. Soc. Edinb. A: Math.*, **77** (1977), 293–308. https://doi.org/10.1017/S030821050002521X
9. C. T. Fulton, Singular eigenvalue problems with eigenvalue parameter contained in the boundary conditions, *Proc. R. Soc. Edinb. A: Math.*, **87** (1980), 1–34. https://doi.org/10.1017/S0308210500012312
10. B. J. Harris, A series solution for certain Ricatti equations with applications to Sturm–Liouville problems, *J. Math. Anal. Appl.*, **137** (1989), 462–470. https://doi.org/10.1016/0022-247X(89)90256-4
11. B. J. Harris, The form of the spectral functions associated with Sturm–Liouville problems with continuous spectrum, *Mathematika*, **44** (1997), 149–161. https://doi.org/10.1112/S0025579300012043
12. A. Kabataş, On eigenfunctions of Hill' s equation with symmetric double well potential, *Commun. Fac. Sci. Univ. Ank. Ser. A1. Math. Stat.*, **71** (2022), 634–649. https://doi.org/10.31801/cfsuasmas.974409
13. A. Kabataş, Sturm–Liouville problems with nonlinear dependence on the spectral parameter in the boundary conditions, *Bound. Value Probl.*, **118** (2025). https://doi.org/10.1186/s13661-025-02086-8

14. N. Y. Kapustin, On the spectral problem arising in the solution of a mixed problem for the heat equation with a mixed derivative in the boundary condition, *Diff. Equat.*, **48** (2012), 701–706. https://doi.org/10.1134/S0012266112050084

15. N. Karjanto, On modified second Paine–de Hoog–Anderssen boundary value problem, *Symmetry*, **14** (2022), 54. https://doi.org/10.3390/sym14010054

16. N. Karjanto, P. Sadhani, Unraveling the complexity of inverting the Sturm–Liouville boundary value problem to its canonical form, *Mathematics*, **12** (2024), 1329. https://doi.org/10.3390/math12091329

17. N. B. Kerimov, K. R. Mamedov, On one boundary value problem with a spectral parameter in the boundary conditions, *Sib. Math. J.*, **40** (1999), 281–290. https://doi.org/10.1007/s11202-999-0008-5

18. P. Lancaster, K. Salkauskas, Surfaces generated by moving least squares methods, *Math. Comput.*, **37** (1981), 141–158. https://doi.org/10.1090/S0025-5718-1981-0616367-1

19. X. Li, A stabilized element-free Galerkin method for the advection–diffusion–reaction problem, *Appl. Math. Lett.*, **146** (2023), 108831. https://doi.org/10.1016/j.aml.2023.108831

20. M. Mandrysz, B. Dybiec, Energetics of single-well undamped stochastic oscillators, *Phys. Rev. E*, **99** (2019), 012125. https://doi.org/10.1103/PhysRevE.99.012125

21. C. Messori, Deep into the water: Exploring the hydro-electromagnetic and quantum electrodynamic properties of interfacial water in living systems, *OALib J.*, **6** (2019), e5435. https://doi.org/10.4236/oalib.1105435

22. W. H. Miller, Periodic orbit description of tunneling in symmetric and asymmetric double-well potentials, *J. Phys. Chem.*, **83** (1979), 960–963. https://doi.org/10.1021/j100471a015

23. F. Zhou, Z. Cao, Q. Shen, Energy splitting in symmetric double-well potentials, *Phys. Rev. A.*, **67** (2003), 062112. https://doi.org/10.1103/PhysRevA.67.062112

24. L. Zhou, J. Wang, X. Li, C. Liu, P. Liu, S. Ren, et al., The magneto-electro-elastic multi-physics coupling element free Galerkin method for smart structures in statics and dynamic problems, *Thin-Walled Struct.*, **169** (2021), 108431. https://doi.org/10.1016/j.tws.2021.108431

AIMS Press